Petrology of samples from the structural lens « C »

The rocks discussed here represent pervasively migmatized garnet-bearing gneisses (P04-47, P04-48, P05-1) and a massive leucosome (P10-9) sampled in part C of the studied outcrop (see Section 4 and Figs. 4 and 9 of the paper). The four samples display a bimodal grain-size distribution where anhydrous mafic porphyroblasts (clinopyroxene and/or garnet), elongate feldspar grains, and polygonal quartz aggregates in subparallel alignment are surrounded by an interconnected microgranular quartz-feldspar matrix. Electron microprobe data on mineral chemistry are given in Tables 1–5 of Supplementary material S2.

Samples P04-47 and P05-1 comprise garnet, clinopyroxene, plagioclase, K-feldspar, biotite, amphibole, quartz, calcite, and accessory rutile, ilmenite, titanite, apatite, allanite, and zircon. Clinopyroxene (1-2 mm) and garnet (1-5 mm) prophyroblasts are anhedral, fractured, and resorbed. Retrogressive replacement of garnet by biotite, and clinopyroxene by amphibole or biotite is common at contacts with the microgranular quartz-feldspar matrix. Garnet and clinopyroxene do not display direct boundaries except for very few cases where the contact is free of secondary minerals (Fig. 1a, b). Inclusions of quartz, plagioclase, K-feldspar, ilmenite, and biotite occur in garnet. Inclusions of quartz, plagioclase, apatite, garnet, calcite, amphibole, and biotite are present in clinopyroxene (Fig. 1b). Garnet porphyroblasts do not show compositional zonation except for a retrogressive decrease of Mg in the resorbed outermost rim (Table 1). Core composition is $Alm_{54-59}Grs_{20-25}Prp_{15-18}Sps_{1-3}Adr_{1-3}$, rim is $Alm_{56-62}Grs_{20-25}Prp_{11-17}Sps_{0-3}Adr_{0-5}$. Clinopyroxene is diopside with a retrogressive decrease of Al, Na, and Ti, and an increase of Ca and Mg toward the rims (Table 2). Amphibole (Table 3) corresponds to the ferropargasite – magnesian hastingsite join (cf. Leake et al. 1997). Biotite replacing clinopyroxene has a higher #Mg (0.53-0.58) compared to biotite replacing garnet (#Mg 0.46-0.51) (Table 4). Large feldspar grains (up to 5-6 mm) of plagioclase An_{15-17} and K-feldspar Or_{85-87} contain antiperthite and perthite (An_{14-20}) exsolutions, respectively (Table 5). The microgranular matrix is dominated by plagioclase (An_{16-21} and Or_{86-90}) (Table 5) with randomly oriented biotite and calcite grains in the vicinity of resorbed garnet and clinopyroxene rims (Fig. 1c). Plagioclase inclusions in garnet (An_{15-16}) and in clinopyroxene (An_{16-18}) fall in the same compositional range. The accessory minerals are abundant in the microgranular matrix. Titanite occurs as single ovoid grains or as rims on ilmenite close to resorbed garnet or clinopyroxene rims.

Sample P04-48 is free of clinopyroxene, amphibole, and calcite. Subhedral to lens-like garnet porphyroblasts (~2 mm) are fractured, partly resorbed, and wrapped in biotite. They host inclusions of quartz, rutile, biotite, and plagioclase (Fig. 1d). Compared to garnets in the clinopyroxene-bearing samples, garnet composition in P04-48 shows a slight almandine enrichment and a similar retrogressive change in the outermost rim (core is $Alm_{56-62}Grs_{17-}$

$_{24}Prp_{13-19}Sps_{1-3}Adr_{0-3}$, rim is $Alm_{59-65}Grs_{17-21}Prp_{12-18}Sps_{2-4}Adr_{1-4}$) (Table 1). Garnet resorption is noticeable along the contacts with microgranular quartz-feldspar aggregates (Fig. 1d). Biotite around resorbed garnet rims and larger biotite flakes that underline the foliation in the matrix have a similar Fe-rich composition (#Mg 0.43-0.47) while biotite inclusions in garnet are enriched in Mg (#Mg 0.52-0.58) (Table 4). Large (1-4 mm) feldspars grains are K-feldspar Or_{84-87} and plagioclase An_{12-14}, the latter with abundant antiperthite exsolutions (Or_{84-88}) (Fig. 1e). In the microgranular matrix, feldspar composition shows larger variations with plagioclase (An_{11-17}) weakly enriched in Ca close to resorbed garnet rims and K-feldspar Or_{85-94} (Table 5). Accessory rutile, allanite, apatite, and zircon occur in the microgranular matrix. Ilmenite accompanies biotite close to resorbed garnet rims.

In sample P10-9, microgranular aggregates of plagioclase An_{12-19} and K-feldspar Or_{90-92} anastomose around quartz lenses and ovoid feldspar grains (0.5-3 mm, plagioclase An_{12-15} and K-feldspar Or_{87-88}) (Table 5), all of them in subparallel alignment. Antiperthite and perthite (An_{10-11}) exsolutions are common in large feldspar grains. Most garnet grains (2-4 mm) are wrapped in biotite associated with microgranular aggregates. Some garnets display euhedral outlines against large plagioclase and quartz grains (Fig. 1f). Garnet composition is $Alm_{62}Grs_{21}Prp_{14}Sps_{1}Adr_{2}$ in the core and, in comparison with the other samples, shows the lowest proportion of pyrope in the outermost rim ($Alm_{63-66}Grs_{18-21}Prp_{10-12}Sps_{1-2}Adr_{2-3}$) (Table 1). The retrogressive compositional change is even more pronounced ($Alm_{70}Grs_{16}Prp_{11}Sps_{1}Adr_{2}$) in garnet-quartz intergrowths (Fig. 1f). Such intergrowths are usually interpreted as a retrograde microstructure related to the crystallization of melt in leucosomes (Waters 2001). Biotite is Fe-rich (#Mg 0.36-0.41) (Table 4). The accessory minerals are allanite, zircon, apatite, titanite, ilmenite, and rutile.

Petrographic observations and mineral chemistry reveal signs of disequilibrium in the samples. This includes the retrograde compositional changes in garnet and clinopyroxene, the unmixing of high temperature solid-solution phases during cooling (perthite and antiperthite exsolutions in large feldspars), and the compositional difference of biotite replacing garnet and clinopyroxene. Consequently, it has been assumed that core compositions of individual phases best reflect the peak metamorphic conditions whereas rim-matrix compositions reflect post-peak reequilibration. The peak assemblage includes the cores of clinopyroxene and/or garnet porphyroblasts, large feldspar grains free of exsolutions, and quartz ± calcite. The post-peak assemblage includes the rims of clinopyroxene and/or garnet, secondary biotite and amphibole, microgranular feldspars, and quartz ± calcite. The growth of biotite and amphibole points to the presence of a H_2O-bearing phase (fluid or melt) during retrogression. The post-peak assemblage was probably formed due to either a back-reaction with melt or a retrograde reaction involving aqueous fluids released from crystallizing melts (e.g., Waters 2001). In all

samples, this assemblage is closely associated with microgranular quartz-feldspar aggregates, indicating dynamic recrystallization after melt crystallization. The occurrence of calcite suggests low water activity during melting and post-peak retrogression, at least in the local environment of the clinopyroxene-bearing gneisses.

Pressure-temperature conditions have been calculated with the winTWQ program (Berman 1991, 2007). Selected results are shown in Figure 2. The peak assemblage in the clinopyroxene-bearing samples yields results in the range of 760-809ºC/16.1-17.8 kbar at XCO_2 0.75-0.83 based on intersections of three independent reactions involving the cores of garnet, clinopyroxene, and large plagioclase grains (Fig. 2a, b). The conditions of early retrogression are estimated on the basis of three independent reactions involving garnet rim, neighbouring secondary biotite, and microgranular feldspar (Fig. 2c, d). Considering all samples, the calculated conditions are 804 ± 33ºC/16.8 ± 1.1 kbar (cf. the grey ellipse) at XCO_2 0.01-0.47, overlapping with the results for the peak assemblage. The conditions of final retrogressive equilibrium have been tested via all possible reactions involving the most retrogressed garnet and clinopyroxene rims, secondary biotite, microgranular plagioclase of the highest An-content, calcite, ilmenite, and titanite. The intersection of five independent reactions yields 743 ± 18ºC/12.2 ± 0.5 kbar at XCO_2 0.74 for sample P04-47 and 739 ± 15ºC/13.7 ± 0.6 kbar at XCO_2 0.70 for sample P05-1 (Fig. 2e, f). All calculations yield very low water activity values of ≤ 0.1.

References

Berman, R.G. (1991). Thermobarometry using multi-equilibrium calculations: a new technique, with petrological applications. *Canadian Mineralogist, 29,* 833-855.

Berman, R.G. (2007). WinTWQ (version 2.3): a software package for performing internally-consistent thermobarometric calculations. *Geological Survey of Canada, Open File 5462,* doi:10.4095/223425.

Leake, B.E., et al. (1997). Nomenclature of amphiboles: Report of the Subcommittee on Amphiboles of the International Mineralogical Association, Commission on New Minerals and Mineral Names. *European Journal of Mineralogy, 9,* 623–651.

Waters, D.J. (2001). The significance of prograde and retrograde quartz-bearing intergrowth microstructures in partially melted granulite-facies rocks. *Lithos, 56,* 97–110.

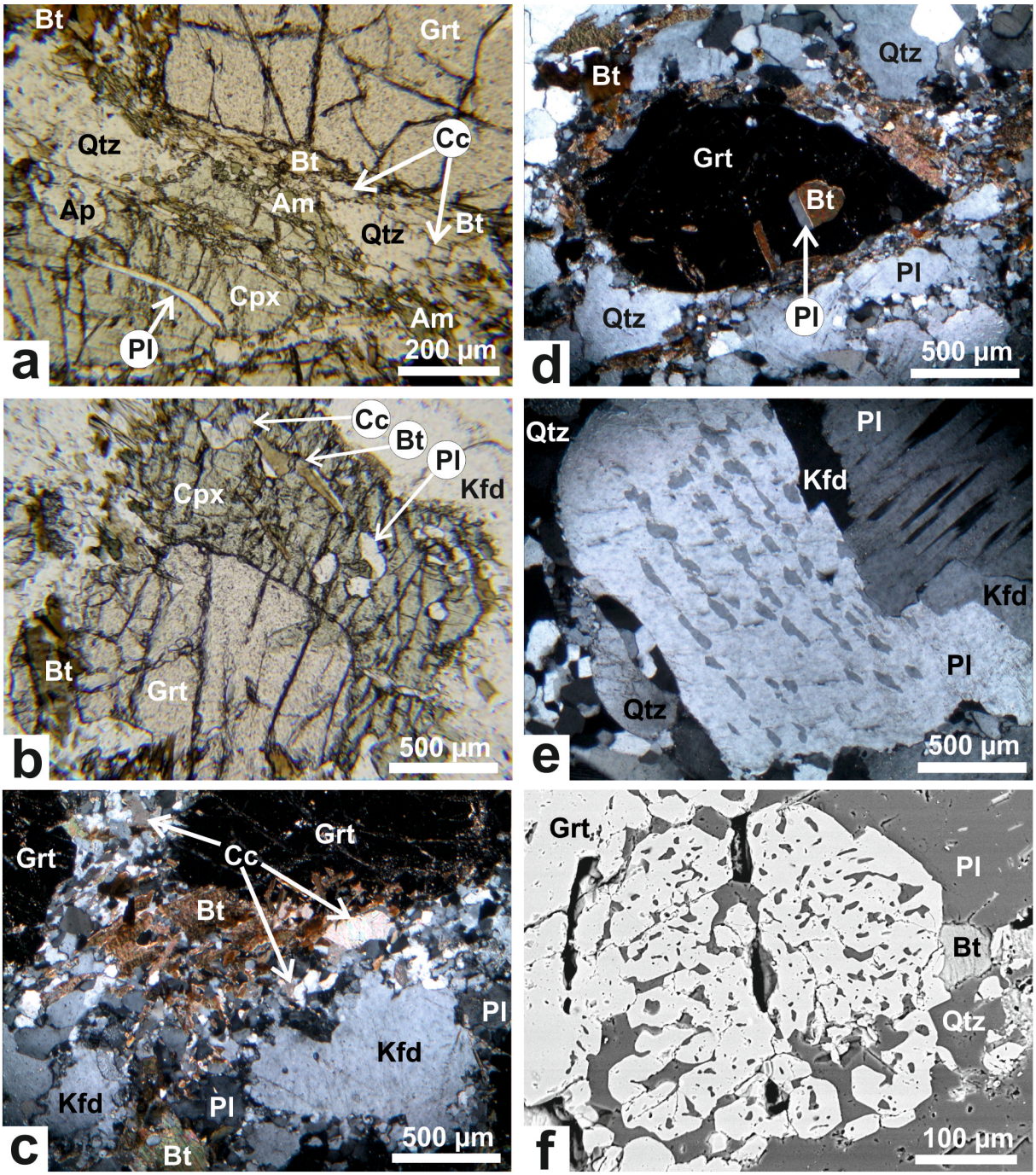

Fig. 1 Photomicrographs (**a–e**) and BSE image (**f**) of samples from the structural lens C. Mineral abbreviations: Am – amphibole; Bt – biotite; Cc – calcite; Cpx – clinopyroxene; Grt – garnet; Kfd – K-feldspar; Pl – plagioclase; Qtz – quartz. **a** Retrogressive replacement of garnet and clinopyroxene by biotite and amphibole in sample P05-1. **b** Garnet-clinopyroxene boundary free of secondary minerals in sample P05-1. **c** Microgranular quartz-feldspar aggregate with biotite and calcite close to resorbed garnet rim in sample P04-47. **d** Anhedral garnet porphyroblast with plagioclase-biotite inclusion and biotite along the rim at contacts with microgranular feldspar aggregates in sample P04-48. **e** Large plagioclase grain with abundant exsolutions of K-feldspar in sample P04-48. **f** Garnet-quartz intergrowths and euhedral garnet outline against large plagioclase and quartz grains in sample P10-9.

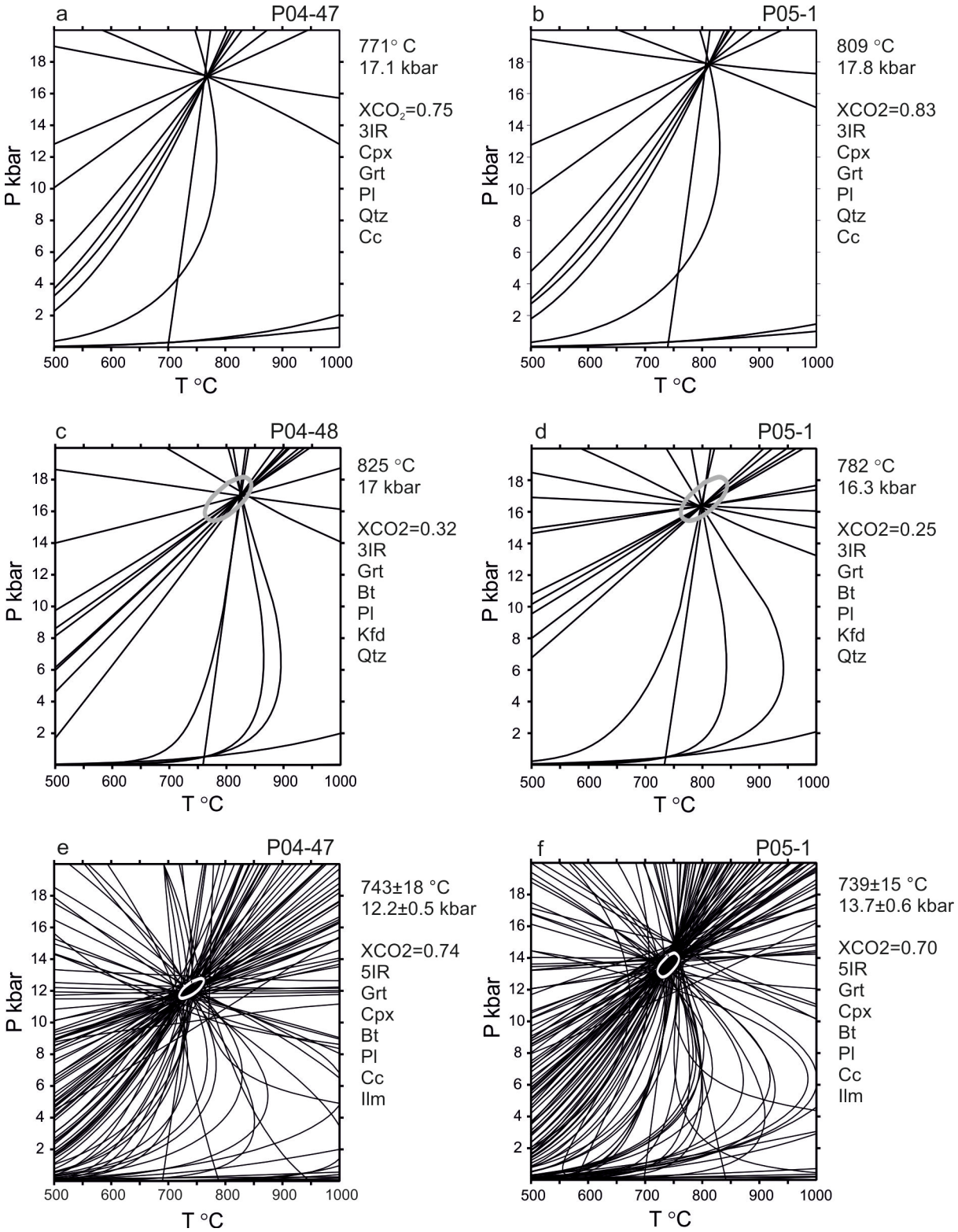

Fig. 2 Selected results of TWQ multi-equilibrium calculations. **a, b** The highest P-T values obtained for the peak assemblage of samples P04-47 and P05-1. The endmembers almandine, grossular, pyrope, diopside, hedenbergite, anorthite (in plagioclase), quartz, calcite, H_2O, and CO_2 were used; the number of independent equilibria is three (3IR). **c, d** P-T results for the assemblages of post-peak interaction in samples P04-48 and P05-1. The endmembers almandine, grossular, pyrope, annite, eastonite, anorthite (in plagioclase), K feldspar, quartz, and H_2O were used; the number of independent equilibria is three (3IR). The grey ellipse outlines the range 804 ± 33ºC/16.8 ± 1.1 kbar reported in the text. **e, f** P-T results for the assemblages of final retrogression in samples P04-47 and P05-1. The endmembers almandine, grossular, pyrope, diopside, annite, phlogopite, eastonite, anorthite (in plagioclase), K feldspar, quartz, calcite, ilmenite, titanite, H_2O, and CO_2 were used; the number of independent equilibria is five (5IR).